

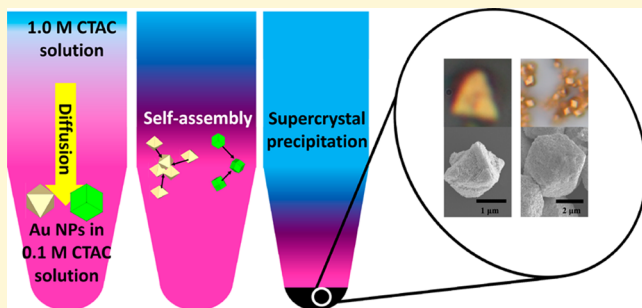
Formation of Free-Standing Supercrystals from the Assembly of Polyhedral Gold Nanocrystals by Surfactant Diffusion in the Solution

Chih-Wen Yang, Chun-Ya Chiu, and Michael H. Huang*

Department of Chemistry, National Tsing Hua University, Hsinchu 30013, Taiwan

Supporting Information

ABSTRACT: Gold supercrystals with polyhedral morphologies can be prepared from the ordered packing of octahedral and rhombic dodecahedral nanocrystals in the presence of a sufficient amount of surfactant by slow water droplet evaporation. The whole supercrystal formation process has been video-recorded using a specially designed chamber to enclose a substrate containing the nanocrystal droplet in a moist environment. Supercrystal growth from the assembly of octahedra is completed within a shorter time. The presence of cetyltrimethylammonium chloride (CTAC) within the supercrystals has been confirmed by small-angle X-ray diffraction analysis. Transmission electron microscopy examination reveals the tendency of two gold octahedra with face contact to fuse, a process frequently observed in the formation of octahedron-assembled supercrystals. Remarkably, we have developed a diffusional surfactant transport approach to make free-standing supercrystals in bulk aqueous solution by adding a concentrated CTAC solution to a concentrated particle solution with a lower CTAC concentration in an Eppendorf tube. Gradual diffusion of CTAC to the lower nanocrystal solution promotes the growth of polyhedral supercrystals. A solution with a sufficiently high surfactant concentration has been shown to be necessary for particle aggregation and supercrystal formation. This method allows the deposition of dense but evenly distributed supercrystals on a substrate. Supercrystals were also used to make a modified electrode for electro-oxidation of glucose. This simple and organic solvent-free approach to making a large quantity of supercrystals allows an ample supply of supercrystals for studies of densely assembled nanocrystal systems and for biomedical applications.



INTRODUCTION

Successful syntheses of polyhedral nanocrystals with controllable morphologies such as cubic, octahedral, and rhombic dodecahedral shapes and uniform sizes have led to observations of their long-range self-assembled structures.^{1–9} Surface modification of nanoparticles with long-chain molecules, surfactant, or polymer promotes their ordered assembly.^{10–28} The control of nanocrystal assembly by changing the solvent used and diffusion of one solvent into another has also been demonstrated.^{29,30} Large supercrystals with polyhedral shapes can be obtained by droplet evaporation of a concentrated nanocrystal solution containing a sufficient amount of surfactant.^{16,17} Having a better understanding of the supercrystal growth process and factors governing their formation is always desirable. Previously, we have assembled gold nanocubes, octahedra, and rhombic dodecahedra to form supercrystals by slow evaporation of a concentrated nanocrystal droplet in a closed vial containing some water to control the evaporation rate.³¹ Transmission X-ray microscopy and optical microscopy were used to follow the supercrystal formation process. Because the optical microscopic observation was made with the evaporating droplet exposed to open air, it would be nice to observe the supercrystal formation process with the droplet placed in a closed and moist environment to simulate

the actual surrounding condition during supercrystal growth. It was also found that the added surfactant mediates particle assembly, and control of its concentration is critical to the formation of high-quality supercrystals. These observations point to the possibility of generating supercrystals directly in the bulk aqueous solution by gradually increasing the surfactant concentration. This concept for the formation of supercrystals or superlattices is new and different from the traditional approaches via evaporation-induced assembly and solvent polarity control. The method avoids the use of organic solvents, and supercrystal growth is no longer confined to a small region of the substrate covered by the droplet.

In this study, we first designed a closed and moist observation chamber to confine the nanocrystal droplet for *in situ* monitoring of the entire supercrystal formation process with an optical microscope. Comparison of the relative growth rates of supercrystals assembled by octahedra and rhombic dodecahedra can be made. Transmission electron microscopy (TEM) examination was conducted to observe the process of fusion between two octahedral particles. X-ray diffraction

Received: July 6, 2014

Revised: August 6, 2014

Published: August 8, 2014



(XRD) patterns were recorded to confirm the presence of the surfactant within a supercrystal. Next, we present a novel diffusional surfactant transport approach for gradually increasing the surfactant concentration in the colloidal solution for the formation of free-standing supercrystals in the bulk solution. The quality of supercrystals obtained by the diffusional approach is also quite good. A substrate can be introduced to grow supercrystals over a large portion of the substrate. The concentration of the surfactant solution was varied to show its effect on particle aggregation. The free-standing supercrystals have been examined for their electrocatalytic activity toward glucose oxidation. The new approach to making supercrystals allows for large-scale production of supercrystals for various applications.

■ EXPERIMENTAL SECTION

Gold Nanocrystal Synthesis. Octahedral and rhombic dodecahedral gold nanocrystals were prepared by a seed-mediated synthesis method described previously.^{1,2} The volume of gold colloidal solution prepared is 10 mL with a cetyltrimethylammonium chloride (CTAC) concentration of 0.1 M. The synthesized gold octahedra have a size range of 39–43 nm (corner–opposite corner distance), while the rhombic dodecahedra have a size range of 52–63 nm (opposite corner distance). Figure S1 of the Supporting Information indicates the particle sizes.

Supercrystal Formation by Droplet Evaporation. The formation of supercrystals by droplet evaporation is similar to that described previously.³¹ First, 10 mL of a 0.1 M CTAC solution was added to the 10 mL solution of gold octahedra. For rhombic dodecahedra, 10 mL of pure water was added to the gold colloid solution to reduce the CTAC concentration to 0.05 M. The resulting solution was centrifuged at 6500 rpm for 10 min. Next, the top solution in the centrifuge tube was carefully removed to leave behind just approximately 50 μ L of the concentrated particle solution. Then 50 μ L of the concentrated colloidal solution was withdrawn and transferred to a small Eppendorf tube. Supercrystals are formed by evaporating the concentrated gold colloid solution slowly in a moist atmosphere using a setup described previously.³¹ First, 1 μ L of the concentrated gold colloidal solution was added to a clean silicon wafer (\sim 5 mm \times 5 mm) or an indium tin oxide (ITO) glass. The substrate was placed over an inverted vial cap, which was placed on top of a 5 mL vial filled with 4 mL of water to prevent the vial from tilting. The 5 mL vial was placed inside a 50 mL vial with 15 mL of water added. The closed vial was placed in an oven set at 90 °C for 12 h to slowly evaporate the droplet for supercrystal formation.

Optical Microscopy Observation. To record the entire supercrystal formation process in a moist environment at room temperature by optical microscopy, a specially designed setup was made (Figure S2 of the Supporting Information). This setup can significantly decrease the droplet evaporation rate to simulate the surrounding environment described above for supercrystal formation, allowing *in situ* observation of the whole process until droplet evaporation in 3 h. Here 0.5 μ L of the gold colloidal solution was added to a clean Si wafer placed over the holder of the observation chamber. The cap was quickly screwed to prevent droplet drying before observation. The whole device was then placed on the microscope sample stage for video recording.

Formation of Free-Standing Supercrystals through a Diffusional Increase in the Surfactant Concentration in the Solution. The concentrated colloidal solution (100 μ L) after centrifugation was left at the bottom of an Eppendorf tube. Then 200 μ L of the 1.0 M CTAC solution was gently introduced without disturbance to keep the CTAC solution and the colloidal solution separated into two layers. This is possible because the density of the CTAC solution is lower than that of the colloidal solution. After 12 h, the red colloidal solution turned colorless and supercrystals formed at the bottom of the tube as a black precipitate. In another procedure, a rectangular Si substrate can be placed in the Eppendorf tube to grow supercrystals directly on the substrate. The substrate was placed in a

slanted position (see Figure S3 of the Supporting Information). Here 500 μ L of the concentrated gold colloidal solution was kept in the tube, and 1.0 mL of the 1.0 M CTAC solution was introduced next.

Electrocatalytic Activity of Au Supercrystals toward Glucose Oxidation. Gold octahedra forming both a monolayer and supercrystals were examined for electrochemical oxidation of glucose. The droplet evaporation method was adopted to form these structures. Here an indium tin oxide (ITO) glass (15 mm \times 50 mm) was used as the substrate for good electrical conductivity. The ITO glass was immersed in ethanol, followed by ultrasonication for 10 min. To fabricate a monolayer of nanocrystals, 2 μ L of the gold colloidal solution was diluted to 40 μ L by adding the 0.1 M CTAC solution, followed by dropping 40 μ L of the dilute solution onto the ITO glass. Supercrystals were formed by directly dropping 2 μ L of the gold colloidal solution onto the ITO glass. The examination of electrocatalytic activity follows the conditions reported previously.³² A Metrohm Autolab GPSTAT 101 electrochemical workstation was used for the electrochemical measurements. The nanocrystal-loaded ITO glass acting as the working electrode was immersed in 100 mL of a solution containing 0.01 M glucose and 0.1 M NaOH. Ag/AgCl was used as the reference electrode, and a platinum wire served as the counter electrode. The ITO glass undergoes an electrochemical treatment by potential cycling between –0.8 and 0.8 V at a scan rate of 50 mV/s.

Instrumentation. Scanning electron microscopy (SEM) was performed using a JEOL JSM-7000F electron microscope. TEM images were obtained using a JEOL JEM-2100 electron microscope. XRD patterns were collected with the use of a Shimadzu XRD-6000 diffractometer with Cu K α radiation. UV-vis absorption spectra were recorded using a JASCO V-670 spectrophotometer.

■ RESULTS AND DISCUSSION

Observation of Supercrystal Formation by Droplet Evaporation. Supercrystals fabricated from the assembly of gold octahedra and rhombic dodecahedra were studied because these building blocks can form high-quality supercrystals with polyhedral shapes. Figure S4 of the Supporting Information gives SEM images of the nice supercrystals formed at 90 °C and schematic drawings of the packing arrangements of nanocrystals in the supercrystals through face contacts. Octahedral gold nanocrystals yield supercrystals having a rhombic dodecahedral morphology. The rhombic dodecahedral supercrystals show different orientations of deposition on the substrate. A monolayer assembly of octahedral nanocrystals is also formed on the substrate. Rhombic dodecahedral nanocrystals are assembled to give supercrystals with a triangular pyramidal shape and a flat top. Truncated triangular supercrystals are also synthesized. Upon close examination of the supercrystals formed through the assembly of gold octahedra, particle fusion can be observed in some supercrystals. Previous observations have shown that particle fusion is more prevalent in supercrystals assembled from gold octahedra; supercrystals constructed from gold nanocubes and rhombic dodecahedra are less prone to fusion.³¹ To provide additional evidence of the tendency of the octahedral gold nanocrystals to fuse, direct observation of the fusion process between two adjacent octahedra was made through TEM examination (see Figure 1). Initially, two octahedra were separated by possibly residual CTAC surfactant. Upon electron beam irradiation for 10 min, the two particles became fused and the gap space was filled through atom migration. Lattice planes of gold appeared in the gap region. It is presumed that the removal of surfactant causes the fusion. Surfactant may be more easily removed between packed gold octahedra during supercrystal formation to promote particle fusion. Fusion is actually less severe when droplet evaporation is performed at 90 °C than at room

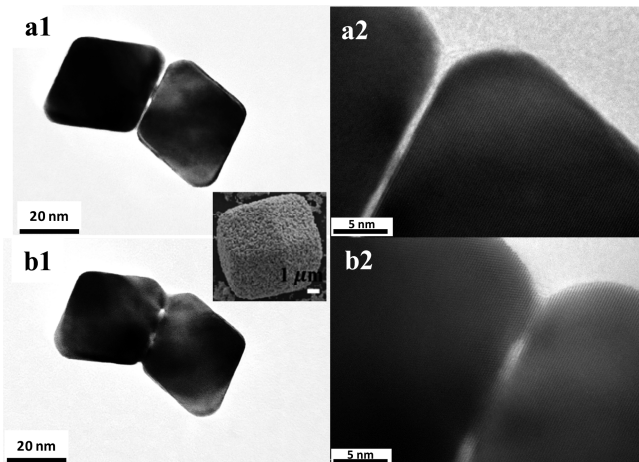


Figure 1. TEM and high-resolution TEM images showing the process of fusion between gold octahedra taken (a1 and a2, respectively) at the very initial moment of TEM observation and (b1 and b2, respectively) after observation for 10 min. These images reveal that the gap between the two contacting particles is gradually disappearing within 10 min of electron beam irradiation. The inset gives a SEM image of a fused supercrystal assembled from gold octahedra.

temperature. Figure S5 of the Supporting Information gives SEM images of unfused rhombic dodecahedral supercrystals formed at 90 °C through the assembly of gold octahedra.

A major purpose of this work is to provide a more complete recording of the entire supercrystal formation process over a large droplet area. Supercrystal or superlattice formation from nanoparticle assembly is a large-scale phenomenon. Recording this process is desirable because such observation is rarely available. In our previous examination of the supercrystal formation process by optical microscopy, the evaporating droplet was exposed to open air.³¹ This may reduce the evaporation time. To better simulate the actual supercrystal formation process, in which the concentrated nanocrystal droplet is placed in a closed and moist environment for slower droplet evaporation, a specially designed chamber for holding the nanocrystal droplet and making optical microscopic observation was constructed (see Figure S2 of the Supporting Information). Water was added inside the chamber, and the droplet was placed very close to the window on top of the chamber for high-magnification optical observation and video recording. Figure 2 offers optical snapshots of the triangular supercrystal formation process taken at different time points after the rhombic dodecahedral nanocrystal droplet was added inside the observation chamber. Movies showing the continuous supercrystal formation process from the assembly of octahedral and rhombic dodecahedral gold nanocrystals are available in the Supporting Information. While a few triangular supercrystals appeared as soon as video recording started, most supercrystals have not grown to be clearly identifiable 14–15 min into the process. Up to this point, the viewing area was still largely purplish red, reflecting the color of a gold colloidal solution. The right side of the viewing area is closer to the edge of the droplet or substrate, and the left side is closer to the central region of the droplet. Figure S6 of the Supporting Information gives an optical image over a large edge region of the substrate, showing the red solution color concentrated toward the inner region of the substrate. Constant and rapid motion can be seen throughout the screen, suggesting extremely dynamic movement of nanoparticles in the droplet.

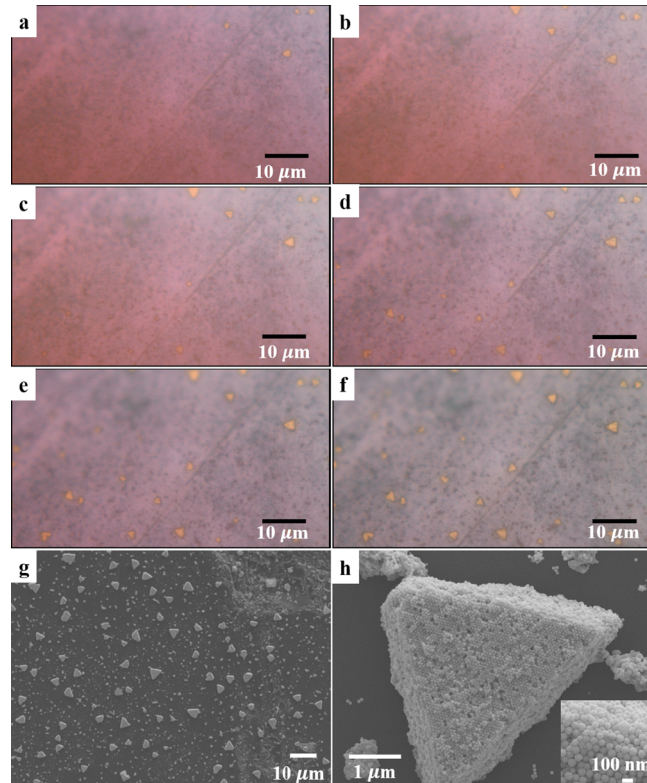


Figure 2. Optical microscopy images of the supercrystal formation process taken at (a) 13, (b) 18, (c) 20, (d) 22, (e) 23, and (f) 28 min time points of the droplet evaporation process. Gold rhombic dodecahedra were used as the building blocks. (g and h) Large-area and enlarged SEM images, respectively, of the synthesized supercrystals. The inset shows a close-up of the assembled rhombic dodecahedra.

The formation of supercrystals only at the right side indicates that supercrystals are first generated at the peripheral or edge region around the droplet. The same observation was made previously.³¹ More than 20 min into the process, small but recognizable supercrystals have appeared throughout the left side of the screen (Figure 2c). Many supercrystals with sizes of ~1 μm quickly grew in the next few minutes via incorporation of the surrounding nanocrystals to evolve into large supercrystals with sizes of ~3 μm more than 28 min into the assembly process. Because of their large dimensions, the supercrystals were fixed to their original positions on the substrate. During this period, the purplish red color gradually faded away from the right side of the screen. The red color continuously moved toward the center of the droplet until the whole substrate lost the red colloidal solution color at 28 min at the point when most of the nanocrystals have been incorporated into the supercrystals. As revealed from the SEM image of the final supercrystals (Figure 2g), the scattered dots seen in the optical image are the tiny assembled structures of nanoparticles. Rhombic dodecahedra can more efficiently pack into three-dimensional structures, so they do not form a monolayer film on the substrate as seen for octahedra. The rhombic dodecahedra still maintain their nice shape in a supercrystal without fusion (Figure 2h). Figure S7 of the Supporting Information presents the selected optical images taken at different time points during the supercrystal formation process using octahedral gold nanocrystals as the building blocks. The entire substrate was still purplish red until the 12

min time point. Many small supercrystals emerged around this time. A monolayer assembly of octahedra grew quickly in size at this time to form a yellowish brown film on the substrate. By 15 min, the monolayer film has covered most of the area of the substrate. The small supercrystals also grew rapidly. By 20 min, supercrystal growth has essentially reached completion. By comparison, the supercrystal formation process is completed within a much shorter time for octahedral nanocrystals than for rhombic dodecahedra.

Supercrystal formation is believed to result from the spontaneous organization of surfactant molecules at a high concentration to form a bilayer structure surrounding the nanocrystals to achieve a state of minimal overall energy.³¹ Given sufficient time for particle assembly, nanocrystals are orderly packed to accommodate the maximal number of surfactant molecules and thereby weaken the overall repulsive electrostatic interactions in a finite volume of solution. In a sense, supercrystal formation and the production of surfactant-templated mesostructured silica involve similar processes.^{33,34} Surfactant-templated mesostructured silica crystals possessing a rhombic dodecahedral shape have also been prepared.^{35,36} To confirm the presence of the CTAC surfactant within the supercrystals, small-angle XRD patterns of supercrystals assembled from octahedra and rhombic dodecahedra were recorded (see Figure 3). The XRD pattern of dried CTAC was also recorded for comparison. Interestingly, although small-angle XRD patterns of rhombic dodecahedral and triangular supercrystals look quite different, both patterns bear some similarity to that of CTAC. To illustrate their similarity, certain peaks having possibly the same origin are connected with

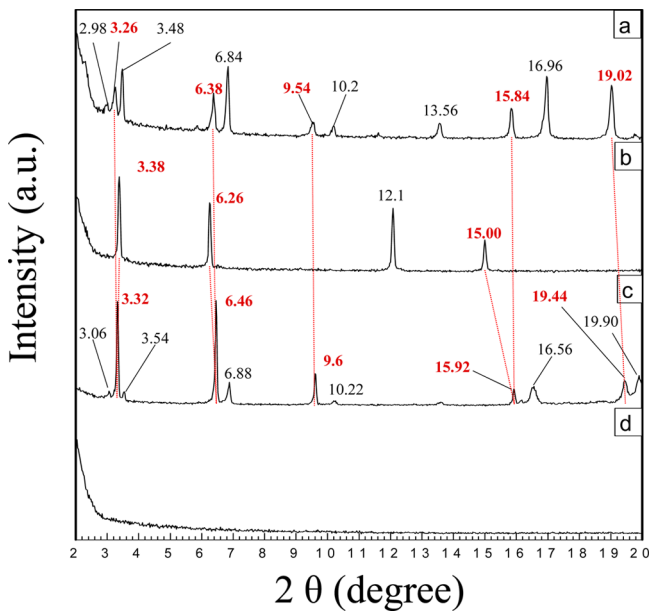


Figure 3. Small-angle XRD patterns of (a) rhombic dodecahedral supercrystals assembled by gold octahedra, (b) triangular supercrystals assembled by gold rhombic dodecahedra, (c) the dried CTAC surfactant, and (d) washed supercrystals to remove the surfactant completely from the supercrystals and the substrate. Supercrystals were produced by the droplet evaporation method. Here 1 mL of deionized water was added to the substrate containing the supercrystals for 10 min. Water and the dissolved CTAC were then removed with a Kimwipe paper. This procedure was performed twice. Peak connections between supercrystals and dried CTAC are marked to indicate extents of peak shift.

dotted lines to show the extents of peak shift. Other than differences in the relative peak intensity and slight shifts in their positions, essentially all the peaks recorded for the rhombic dodecahedral supercrystals are present in the XRD pattern of CTAC. The first two reflection peaks recorded for the triangular supercrystals are also present in CTAC. The peak at 15.00° may be linked to the peak at 15.92° for the dried CTAC. Furthermore, when the surfactant was removed when supercrystals of both shapes were washed with water, all the signature peaks of CTAC disappeared (Figure 3d). The results provide convincing evidence of the presence of the CTAC surfactant within the supercrystals.

Supercrystal Formation by the Surfactant Diffusion Approach.

Because a sufficient amount of surfactant is necessary to promote the formation of supercrystals, we considered the possibility of directly growing supercrystals in bulk solution by gradually increasing the surfactant concentration. In a concentrated nanocrystal solution containing 0.1 M CTAC, additional 1.0 M CTAC solution was added on top of the colloidal solution. Because the CTAC solution is less dense, the two solutions form two layers in an Eppendorf tube (see Figure 4). The surfactant should slowly diffuse from the upper

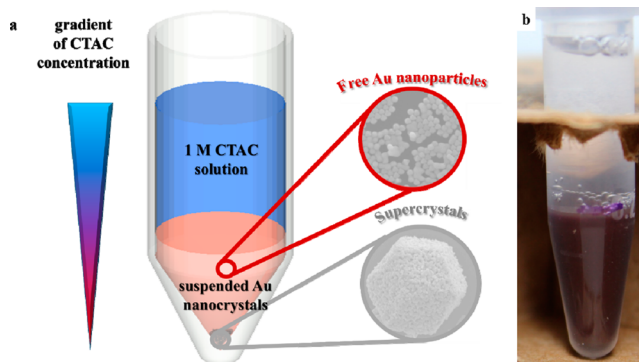


Figure 4. (a) Schematic drawing of the diffusional transport of the CTAC surfactant from the upper layer solution to the lower Au nanocrystal solution to form supercrystals that eventually settle to the bottom of the vial. (b) Photograph of the vial showing the upper concentrated CTAC solution and the lower Au nanocrystal solution. The vial is inserted into a cardboard box.

layer to the lower layer to establish a concentration equilibrium. Over a period of 12 h, the initially dark purple solution of suspended Au particles became clear, and a black precipitate was observed at the bottom of the tube. The disappearance of the colloidal solution color infers that the suspended nanocrystals have aggregated to form a precipitate under the influence of diffusional transport of the surfactant to the lower layer. Figure 5 shows optical and SEM images of the precipitate collected. Remarkably, both the octahedral and rhombic dodecahedral gold nanocrystals have formed numerous supercrystals. Similar rhombic dodecahedral supercrystals were produced from the assembly of octahedra with sizes ranging from <1 to ~4 μm. Octahedral supercrystals with similar sizes were generated from the assembly of rhombic dodecahedra. Because of their large dimensions, the supercrystals display a metallic golden luster when viewed under an optical microscope. The successful growth of supercrystals demonstrates the diffusional surfactant transport method as a simple approach to producing a large quantity of supercrystals, and supercrystal formation is no longer limited to the small volume of a

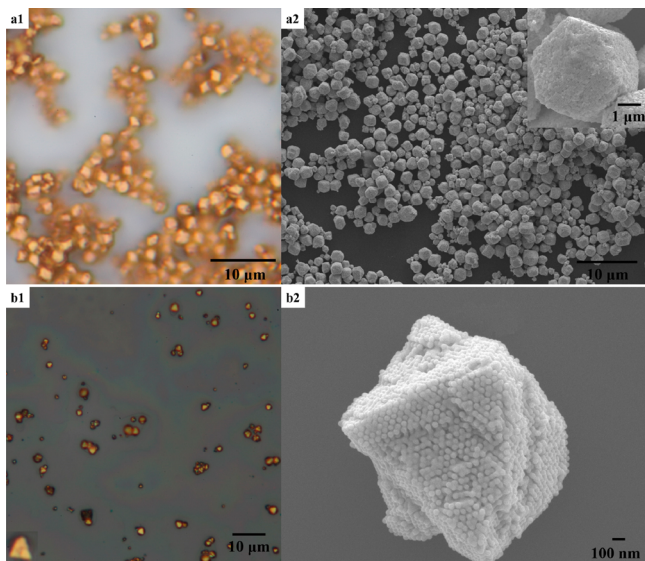


Figure 5. Optical and SEM images of supercrystals formed by the diffusional surfactant transport method. (a1 and a2) Optical and SEM images, respectively, of rhombic dodecahedral supercrystals assembled by octahedral Au nanocrystals. (b1 and b2) Optical and SEM images, respectively, of octahedral supercrystals assembled by Au rhombic dodecahedra. The inset shows a higher-magnification view of a supercrystal.

nanocrystal droplet. This demonstration also shows that solvent evaporation as the main entropy-driving force is not necessary to induce particle assembly; a solution with sufficiently concentrated nanoparticles and surfactant molecules can spontaneously lead to organized packing of nanocrystals given sufficient time. This approach also offers the advantage of using only water as the medium. A mixture of organic solvents is not required, facilitating the use of supercrystals for biomedical applications.

To confirm that a solution with a sufficiently high surfactant concentration can induce particle assembly, Au rhombic dodecahedra and octahedra were added to an aqueous CTAC solution with different surfactant concentrations. Particle aggregation can be followed by detecting a significant spectral red-shift due to extensive coupling of surface plasmon resonance (SPR) of the gold nanocrystals. Figure 6 presents time-dependent UV-vis spectra of rhombic dodecahedral Au nanocrystals dispersed in 0.3 and 0.15 M CTAC solutions. At a CTAC concentration of 0.3 M, the SPR absorption band of dispersed Au rhombic dodecahedra at 550 nm becomes progressively red-shifted over time. After 12 min, the absorption feature becomes very broad and has reached the near-infrared region beyond 1000 nm. This broad absorption over the visible light region is what gives the supercrystal precipitate a black appearance. The absorption profile is essentially unchanged after this point. The absorbance decreases continuously as a result of particle sedimentation because of aggregation. The SEM image shows that the particles are indeed aggregated but do not form polyhedral supercrystals. When the solution was sonicated after 2 h, the initial spectrum returned because of redispersion of nanocrystals in the solution. Interestingly, the use of a CTAC concentration of 0.15 M did not lead to any spectral change as a function of time, indicating that the presence of a sufficient amount of surfactant in the solution is necessary for particle assembly and supercrystal formation. Time-dependent UV-vis

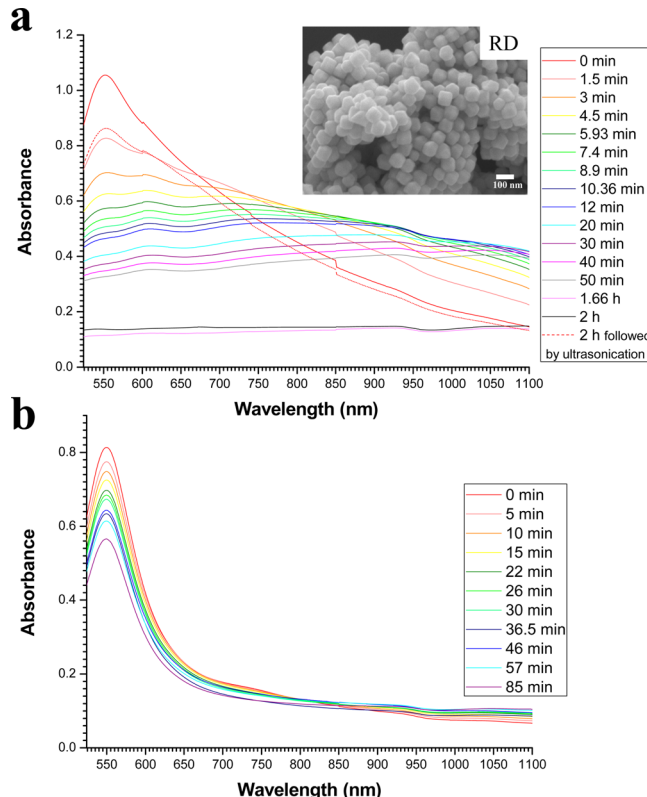


Figure 6. Time-dependent UV-vis absorption spectra of rhombic dodecahedral Au nanocrystals dispersed in (a) 0.3 and (b) 0.15 M CTAC solutions. The inset shows the SEM image of the aggregated rhombic dodecahedra in a 0.3 M CTAC solution.

spectra of gold octahedra in 0.3 and 0.7 M CTAC solutions were also recorded (Figure S6 of the Supporting Information). The same spectral red-shift was observed, although the broad absorption band feature appears more rapidly at a higher CTAC concentration. It is interesting to note that at the same CTAC concentration of 0.3 M, octahedra have essentially aggregated within 4 min, while it took rhombic dodecahedra 10–12 min to do this. This relative particle aggregation rate is consistent with the observation of gold octahedra completing the supercrystal growth within a much shorter time. The results show that polyhedral supercrystals are produced only by a slow diffusional increase in the surfactant concentration in the solution; direct and rapid introduction of a large quantity of surfactant yields only less ordered packing of nanocrystals. Ordered surfactant organization between nanocrystals takes time. Similarly, mesostructured silica with surfactant micelles as templates does not form instantly after the reagents are mixed. The use of a cetyltrimethylammonium bromide (CTAB) surfactant can also produce supercrystals (data not shown). On the basis of the observations described above, we found the general notion of depletion attraction or force often used to describe colloidal particle self-assembly is not very useful here, even though it can be considered that surfactant micelles present in the solution can induce an attractive force to pull particles together.^{37–39} First, other than surfactant, no additives have been added. Surfactant is typically introduced during nanocrystal growth, and a relatively low concentration of surfactant, but still well above the critical micelle concentration of CTAC at 0.8 mM,^{39,40} does not lead to supercrystal formation as shown in this study. Furthermore, the depletion

attraction mechanism does not explain why the surfactant packing arrangement in supercrystals is similar to that of dried CTAC as seen in the XRD patterns, meaning that surfactant molecules are densely packed in an orderly fashion between contacting nanocrystals within a supercrystal. It also cannot explain why polyhedron-constructed supercrystals with geometrically symmetric shapes are produced, the very large sizes of these supercrystals, and the time it takes to form good supercrystals. However, the conventional understanding of surfactant interactions can explain all these results.

Because supercrystals are formed in the bulk solution before settling to the bottom of the Eppendorf tube, a rectangular-shaped Si substrate can be loaded inside the tube to collect the supercrystals (Figure S7 of the Supporting Information). Small supercrystals were collected at the upper portion of the substrate, while larger supercrystals were deposited near the bottom of the substrate; therefore, rough size sorting of supercrystals was achieved this way. Figure 7 gives SEM and

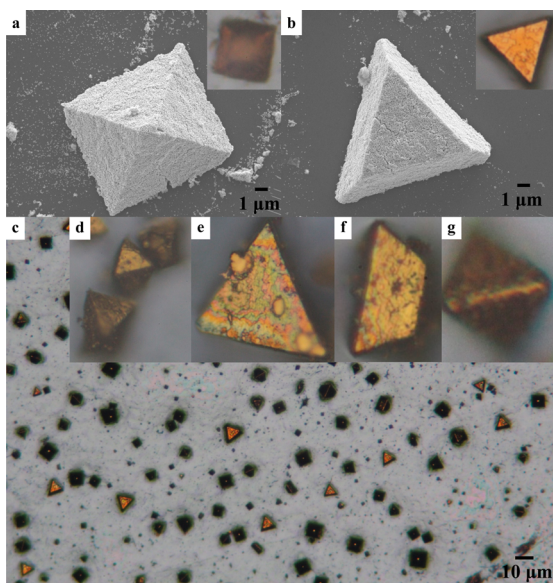


Figure 7. (a and b) SEM images of square pyramidal and triangular pyramidal supercrystals, respectively, formed on a substrate using the diffusional surfactant transport method. Rhombic dodecahedral Au nanocrystals were used as the building blocks. Insets show their representative optical microscopic images. (c) Optical micrograph over a very large area of the substrate to show the well-distributed formation of supercrystals. (d–g) High-magnification optical images of individual supercrystals with different shapes and orientations.

optical microscopic images of supercrystals grown on a Si wafer from the assembly of gold rhombic dodecahedra. In addition to the observation of octahedral supercrystals, which should be formed in the solution before they land on the substrate, square pyramidal and triangular pyramidal supercrystals were observed on the substrate. These structures can be constructed only through direct growth on a substrate. Nicely, the supercrystals are well-scattered over the entire substrate, so ultralarge-area deposition of evenly distributed supercrystals is possible. The substrate surface is also relatively clean. This simple method of growing supercrystals on a substrate is superior to our previous approach of removing supercrystals grown by droplet evaporation with a NaOH solution and transferring them to another substrate.³¹

Electrocatalytic Activity of Au Supercrystals. Compared to supercrystals assembled from rhombic dodecahedra, supercrystals produced from the assembly of octahedra naturally contain larger pores and possibly more channel spaces (see Figure S4 of the Supporting Information). Supercrystals should act as a modified electrode because they can be deposited on an electrode surface. It is interesting to examine the electrocatalytic activity of supercrystals. Here 2 μL of Au octahedron droplet-forming supercrystals was deposited on an ITO electrode for electrochemical oxidation of glucose. For comparison, the same amount of a Au octahedron droplet (but much diluted) forming a monayer of assembled particle film on an ITO electrode was also tested. Figure 8 displays

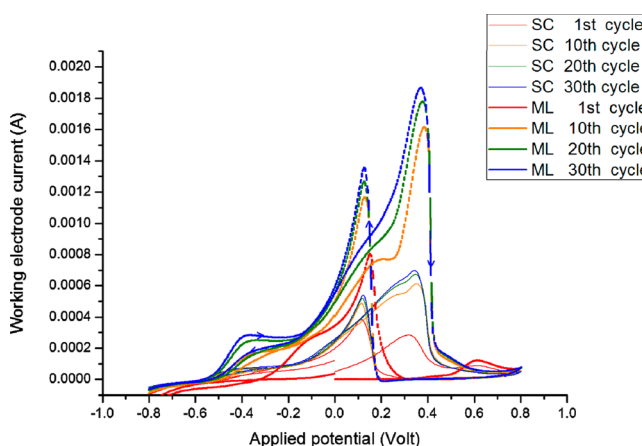


Figure 8. Cyclic voltammograms of supercrystals (SC) and a monolayer (ML) film assembled from octahedral gold nanocrystals on an ITO glass electrode in a solution containing 0.1 M NaOH and 0.01 M glucose. The scan rate is 50 mV/s.

cyclic voltammograms (CV) of supercrystals and a monolayer film assembled from octahedral gold nanocrystals in a solution containing 0.1 M NaOH and 0.01 M glucose. There are large peak shifts in the CV curves between the first scan and the 10th scan. The peak positions then became more stabilized, and higher currents were recorded after 30 scan cycles. A typical two-step oxidation process was observed. The first oxidation peak at -0.40 V in the positive scan results from the oxidation of glucose to gluconolactone, while the second oxidation peaks at 0.35 and 0.37 V for the supercrystals and monolayer film, respectively, correspond to further oxidation of gluconolactone.^{32,41} In the negative scan, a reduction peak appears at 0.12 V for both samples. Obviously, the oxidation current is much higher for the monolayer film than for the supercrystals (~ 2.65 times higher). The monolayer film makes many more contacts with the electrode surface, so it is reasonable that the film exhibits superior electrocatalytic performance. Nevertheless, supercrystals can still serve as an effective modified electrode, especially if they can be more densely deposited on the electrode surface.

CONCLUSIONS

The whole process for the formation of supercrystals assembled from octahedral and rhombic dodecahedral gold nanocrystals by droplet evaporation has been captured using a specially designed chamber to decrease the evaporation rate. Octahedral nanocrystals complete the supercrystal growth process much more quickly. The presence of the CTAC surfactant within

supercrystals has been confirmed by taking XRD patterns of supercrystals. TEM examination reveals octahedral gold nanocrystals are prone to fusion when they are in close contact. Most importantly, this work demonstrates a new approach to making a large quantity of free-standing supercrystals by introducing a more concentrated CTAC solution to a concentrated gold nanocrystal solution with a lower surfactant concentration. Diffusional transport of the surfactant to the lower nanoparticle layer promotes the production of polyhedral supercrystals. Using this method, a large amount of supercrystals can form on a substrate, so a large-scale deposition of evenly distributed supercrystals on a substrate can be achieved. The control of surfactant concentration in the bulk solution has been shown to be essential for particle aggregation and supercrystal formation. Electrochemical oxidation of glucose using a supercrystal-modified electrode has been demonstrated. It is expected that this diffusional method of making supercrystals in an aqueous solution should offer an ample supply of supercrystals for examination of various properties of highly assembled nanoparticle systems.

■ ASSOCIATED CONTENT

S Supporting Information

Illustration of the setup used for optical microscopy observation, illustration of supercrystal growth on a substrate by the diffusional method, additional SEM images of supercrystals, optical microscopic images of the supercrystal formation process, UV-vis spectra of gold octahedra in a CTAC solution, and movies showing the continuous supercrystal formation process from the assembly of octahedral and rhombic dodecahedral gold nanocrystals. This material is available free of charge via the Internet at <http://pubs.acs.org>.

■ AUTHOR INFORMATION

Corresponding Author

*E-mail: hyhuang@mx.nthu.edu.tw.

Notes

The authors declare no competing financial interest.

■ ACKNOWLEDGMENTS

We thank the Ministry of Science and Technology of Taiwan for support of this research (NSC 101-2113-M-007-018-MY3 and NSC 102-2633-M-007-002).

■ REFERENCES

- Wu, H.-L.; Kuo, C.-H.; Huang, M. H. *Langmuir* **2010**, *26*, 12307–12313.
- Chung, P.-J.; Lyu, L.-M.; Huang, M. H. *Chem.–Eur. J.* **2011**, *17*, 9746–9752.
- Chang, C.-C.; Wu, H.-L.; Kuo, C.-H.; Huang, M. H. *Chem. Mater.* **2008**, *20*, 7570–7574.
- Langille, M. R.; Personick, M. L.; Zhang, J.; Mirkin, C. A. *J. Am. Chem. Soc.* **2012**, *134*, 14542–14554.
- Niu, Z.; Peng, Q.; Gong, M.; Rong, H.; Li, Y. *Angew. Chem., Int. Ed.* **2011**, *50*, 6315–6319.
- Kang, Y.; Pyo, J. B.; Ye, X.; Diaz, R. E.; Gordon, T. R.; Stach, E. A.; Murray, C. B. *ACS Nano* **2013**, *7*, 645–653.
- Tsao, Y.-C.; Rej, S.; Chiu, C.-Y.; Huang, M. H. *J. Am. Chem. Soc.* **2014**, *136*, 396–404.
- Wu, J.-K.; Lyu, L.-M.; Liao, C.-W.; Wang, Y.-N.; Huang, M. H. *Chem.–Eur. J.* **2012**, *18*, 14473–14478.
- Chiu, C.-Y.; Yang, M.-Y.; Lin, F.-C.; Huang, J.-S.; Huang, M. H. *Nanoscale* **2014**, *6*, 7656–7665.
- Zhang, J.; Luo, Z.; Quan, Z.; Wang, Y.; Kumbhar, A.; Smilgies, D.-M.; Fang, J. *Nano Lett.* **2011**, *11*, 2912–2918.
- Tao, A. R.; Ceperley, D. P.; Sinsermsuksakul, P.; Neureuther, A. R.; Yang, P. *Nano Lett.* **2008**, *8*, 4033–4038.
- Bishop, K. J. M.; Wilmer, C. E.; Soh, S.; Gryzbowski, B. A. *Small* **2009**, *5*, 1600–1630.
- Quan, Z.; Fang, J. *Nano Today* **2010**, *5*, 390–411.
- Zhu, Z.; Meng, H.; Liu, W.; Liu, X.; Gong, J.; Qiu, X.; Jiang, L.; Wang, D.; Tang, Z. *Angew. Chem., Int. Ed.* **2011**, *50*, 1593–1596.
- Nakagawa, Y.; Kageyama, H.; Oaki, Y.; Imai, H. *J. Am. Chem. Soc.* **2014**, *136*, 3716–3719.
- Xie, S.; Zhou, X.; Han, X.; Kuang, Q.; Jin, M.; Jiang, Y.; Xie, Z.; Zheng, L. *J. Phys. Chem. C* **2009**, *113*, 19107–19111.
- Zhao, Z.; Zhang, J.; Dong, F.; Yang, B. *J. Colloid Interface Sci.* **2011**, *359*, 351–358.
- Shen, X. S.; Wang, G. Z.; Hong, X.; Zhu, W. *CrystEngComm* **2009**, *11*, 753–755.
- Demortière, A.; Launois, P.; Goubet, N.; Albouy, P.-A.; Petit, C. *J. Phys. Chem. B* **2008**, *112*, 14583–14592.
- Sau, T. K.; Murphy, C. J. *Langmuir* **2005**, *21*, 2923–2929.
- Henzie, J.; Grünwald, M.; Widmer-Cooper, A.; Geissler, P. L.; Yang, P. *Nat. Mater.* **2012**, *11*, 131–137.
- Ming, T.; Kou, X.; Chen, H.; Wang, T.; Tam, H.-L.; Cheah, K.-W.; Chen, J.-Y.; Wang, J. *Angew. Chem., Int. Ed.* **2008**, *47*, 9685–9690.
- Shevchenko, E. V.; Talapin, D. V.; Kotov, N. A.; O'Brien, S.; Murray, C. B. *Nature* **2006**, *439*, 55–59.
- Redl, F. X.; Cho, K.-S.; Murray, C. B.; O'Brien, S. *Nature* **2003**, *423*, 968–971.
- Chen, C.-F.; Tzeng, S.-D.; Chen, H.-Y.; Lin, K.-J.; Gwo, S. *J. Am. Chem. Soc.* **2008**, *130*, 824–826.
- Bodnarchuk, M. I.; Kovalenko, M. V.; Heiss, W.; Talapin, D. V. *J. Am. Chem. Soc.* **2010**, *132*, 11967–11977.
- Xie, Y.; Guo, S.; Guo, C.; He, M.; Chen, D.; Ji, Y.; Chen, Z.; Wu, X.; Liu, Q.; Xie, S. *Langmuir* **2013**, *29*, 6232–6241.
- Chen, C.-J.; Chiang, R.-K.; Jeng, Y.-R. *J. Phys. Chem. C* **2011**, *115*, 18142–18148.
- Quan, Z.; Xu, H.; Wang, C.; Wen, X.; Wang, Y.; Zhu, J.; Li, R.; Sheehan, C. J.; Wang, Z.; Smilgies, D.-M.; Luo, Z.; Fang, J. *J. Am. Chem. Soc.* **2014**, *136*, 1352–1359.
- Talapin, D. V.; Shevchenko, E. V.; Kornowski, A.; Gaponik, N.; Haase, M.; Rogach, A. L.; Weller, H. *Adv. Mater.* **2001**, *13*, 1868–1871.
- Liao, C.-W.; Lin, Y.-S.; Chanda, K.; Song, Y.-F.; Huang, M. H. *J. Am. Chem. Soc.* **2013**, *135*, 2684–2693.
- (a) Tominaga, M.; Shimazoe, T.; Nagashima, M.; Kusuda, H.; Kubo, A.; Kuwahara, Y.; Taniguchi, I. *Electroanal. Chem.* **2006**, *590*, 37–46. (b) Tominaga, M.; Shimazoe, T.; Nagashima, M.; Taniguchi, I. *Electrochim. Commun.* **2005**, *7*, 189–193.
- Raman, N. K.; Anderson, M. T.; Brinker, C. J. *Chem. Mater.* **1996**, *8*, 1682–1701.
- Chen, P.-K.; Lai, N.-C.; Ho, C.-H.; Hu, Y.-W.; Lee, J.-F.; Yang, C.-M. *Chem. Mater.* **2013**, *25*, 4269–4277.
- Gu, D.; Bongard, H.; Meng, Y.; Miyasaka, K.; Terasaki, O.; Zhang, F.; Deng, Y.; Wu, Z.; Feng, D.; Fang, Y.; Tu, B.; Schüth, F.; Zhao, D. *Chem. Mater.* **2010**, *22*, 4828–4833.
- Xia, Y.; Mokaya, R. *J. Mater. Chem.* **2003**, *13*, 657–659.
- Baranov, D.; Fiore, A.; van Huis, M.; Giannini, C.; Falqui, A.; Lafont, U.; Zandbergen, H.; Zanella, M.; Cingolani, R.; Manna, L. *Nano Lett.* **2010**, *10*, 743–749.
- Zhang, S.-Y.; Regulacio, M. D.; Han, M.-Y. *Chem. Soc. Rev.* **2014**, *43*, 2301–2323.
- Young, K. L.; Personick, M. L.; Engel, M.; Damasceno, P. F.; Barnaby, S. N.; Bleher, R.; Li, T.; Glotzer, S. C.; Lee, B.; Mirkin, C. A. *Angew. Chem., Int. Ed.* **2013**, *52*, 13980–13984.
- Roelants, E.; De Schryver, F. C. *Langmuir* **1987**, *3*, 209–214.
- Wang, J.; Gong, J.; Xiong, Y.; Yang, J.; Gao, Y.; Liu, Y.; Lu, X.; Tang, Z. *Chem. Commun.* **2011**, *47*, 6894–6986.